MATERIALS SCIENCE

Local symmetry predictors of mechanical stability in glasses

Amelia C. Y. Liu[1,2]*, Espen D. Bøjesen[1,3], Rico F. Tabor[4], Stephen T. Mudie[5], Alessio Zaccone[6], Peter Harrowell[7], Timothy C. Petersen[1,2]

The mechanical properties of crystals are controlled by the translational symmetry of their structures. But for glasses with a disordered structure, the link between the symmetry of local particle arrangements and stability is not well established. In this contribution, we provide experimental verification that the centrosymmetry of nearest-neighbor polyhedra in a glass strongly correlates with the local mechanical stability. We examine the distribution of local stability and local centrosymmetry in a glass during aging and deformation using microbeam x-ray scattering. These measurements reveal the underlying relationship between particle-level structure and larger-scale behavior and demonstrate that spatially connected, coordinated local transformations to lower symmetry structures are fundamental to these phenomena. While glassy structures lack obvious global symmetry breaking, local structural symmetry is a critical factor in predicting stability.

INTRODUCTION

In crystals, mechanical deformation is mediated by the creation and propagation of topological defects, which are precisely defined discontinuities in the translational symmetry. In contrast, glasses have a continuum of local configurations (*1*), and the identity of zones that will undergo transformation under load in glasses cannot yet be predicted on a structural basis, although many structural indicators have been found to correlate with a propensity for plastic activity (*2*–*4*). It is an ongoing materials engineering challenge to understand the identity, size, and spatial distribution of these zones and how they transform and interact to produce the global phenomena of aging, embrittlement, rejuvenation, and plasticity in glasses (*5*). A critical idea in understanding elasticity in glasses is the nonaffine component of their response to applied force (*3*, *4*, *6*–*11*). In centrosymmetric crystals, each particle is a center of symmetry, that is, any pair of opposing nearest neighbors is placed such that a straight line drawn through the particle will intersect these neighbors at the same distance from the center. The pair of nearest neighbors is related by mirror symmetry or inversion symmetry about the central particle. In this case, the force applied to any one particle is balanced by its neighbors, and the particles undergo affine displacements that are proportional to the applied force until the elastic limit is reached, and topological defects are created. In dense glasses with isotropic interparticle interactions, such as those considered in this work, each particle is in a unique local environment, and simultaneously the center of its own nearest-neighbor polyhedron and vertex of adjacent polyhedra. These nearest-neighbor configurations may correspond to a distinct polyhedral type from a broad diversity but, at the same time, generally contain disorder or distortion (*1*). The potential imbalance of forces on any given particle results in nonaffine displacements, that, overall, reduce the energy of deformation and material stiffness (*8*, *9*).

These nonaffine displacements in an amorphous material are highly localized and excellent identifiers of irreversible transformations (*11*). They also correlate with a "softness" parameter derived from machine learning that uses a large set of structural parameters to predict the probability of particle rearrangements (*3*, *4*). In jammed packings, only a proportion of all point contact changes are associated with these irreversible transformations (*12*). In another approach to understanding the relationship of structure to stability in glasses, the local particle geometry is specifically encoded into the material response (*6*, *8*, *9*), whereby the nonaffine displacements of particles are due to the sum of forces from nearest neighbors ($\boldsymbol{f}$) as in Eq. 1.

$$\boldsymbol{f}_i = \boldsymbol{\Xi}_i \gamma \tag{1}$$

Here, γ is the strain, and $\boldsymbol{\Xi}_i$ is a vector that quantifies the degree of centrosymmetry and, thus, force imbalance around the ith particle (*6*, *8*, *9*). The shear modulus of the material, reflecting stiffness, is then composed of an affine (G_A) and nonaffine (G_{NA}) contribution.

$$G = G_A - G_{NA} \tag{2}$$

G_{NA} is a function of $\boldsymbol{\Xi}_i$ and the Hessian (positive in the vicinity of a global energy minimum), and thus, the nonaffine displacements reduce the modulus. $\boldsymbol{\Xi}_i$ encapsulates the local structural symmetry, and is a fluctuating, short-range vector field, with much apparent randomness as would be anticipated for a glass. On the other hand, the nonaffine displacements that are the linear response to these forces show much longer-range correlations, cooperativity, and large swirling, vortex-like structures (*8*, *9*). In this way, $\boldsymbol{\Xi}_i$ and nonaffine displacements provide the key connection between apparently random, fluctuating local structure and the longer-range cooperative behaviors that are observed in glasses.

In this study, we make a direct link between local stability and local structural symmetry in a glass using x-ray scattering microscopy (Fig. 1). Our measured maps of structure and softness demonstrate that the local degree of centrosymmetry is a strong predictor for mechanical stability in glasses. Furthermore, we examine glass

[1]Monash Centre for Electron Microscopy, Monash University, Clayton, Victoria, 3800, Australia. [2]School of Physics and Astronomy, Monash University, Clayton, Victoria, 3800, Australia. [3]Interdisciplinary Nanoscience Centre and Centre for Integrated Materials Research, Aarhus University, Aarhus C 8000, Denmark. [4]School of Chemistry, Monash University, Clayton, Victoria 3800, Australia. [5]Australian Synchrotron, ANSTO, Clayton, Victoria 3168, Australia. [6]Department of Physics, University of Milan, Milan, Italy. [7]School of Chemistry, University of Sydney, Sydney, N.S.W. 2006, Australia.
*Corresponding author. Email: amelia.liu@monash.edu

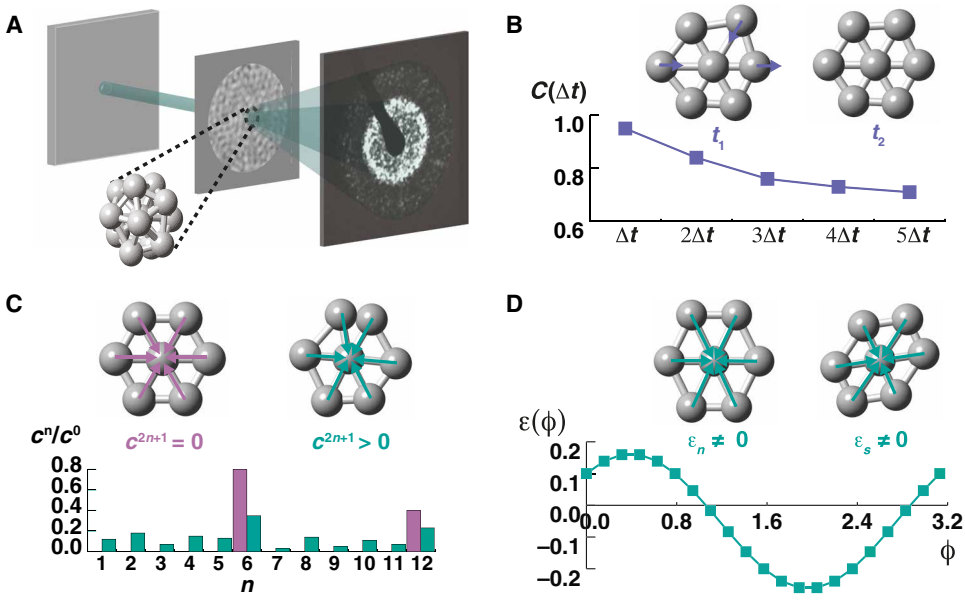

Fig. 1. μSAXS as a probe of local structure in a colloidal glass. (**A**) Geometry of scanning μSAXS in which the size of the illuminating beam is comparable to the size of the nearest-neighbor polyhedral cluster. The corresponding diffraction pattern is not composed of smooth, isotropic rings, but discrete speckles that reflect local structure. (**B**) Local stability is probed from the time correlation coefficient [$C(\Delta t)$] between consecutive μSAXS patterns. (**C**) Degree of local centrosymmetry is reflected in the magnitude of odd-order angular symmetries in the μSAXS pattern ($c^{2n+1} > 0$). (**D**) Local structural anisotropy (ϵ_n and ϵ_s) can be quantified from fitting the anisotropy in the μSAXS pattern with an anisotropy function [$\epsilon(\phi)$]. In the figure, bonds are drawn to emphasize the symmetry of particle arrangements.

aging and deformation and find that coordinated local structural transformations to lower symmetry structures are at the heart of these phenomena, providing particle-level insight into aging and embrittlement (*5*, *13*, *14*) and deformation-induced localization of strain in "shear bands" (*13*, *15*, *16*).

Scanning x-ray microscopy to map local stability and local structure

The identification and prediction of soft zones in glasses and disordered packings has so far been accomplished using atomistic models (*3*, *4*, *8*, *9*, *11*), confocal optical and video microscopy of microspheres (*13*, *17*–*21*), or photoelasticimetry (*22*), where particle positions can be tracked in three dimensions as a function of strain and time. Here, we demonstrate an experimental scanning x-ray microscopy to map local stability and local structure in a glass that does not require volumetric reconstruction of particle positions. The experimental geometry is shown in Fig. 1A; a thin, colloidal glass specimen [300-nm-diameter spherical SiO_2 with 5% polydispersity (*23*)] is scanned in an x-ray microbeam, and a transmission micro–small-angle x-ray scattering (μSAXS) pattern is collected at each point. These "speckle" diffraction patterns contain rich information that probes local structures (*23*–*25*). Here, we simultaneously extract three parameters from each μSAXS pattern that together provide fresh understanding of the relationship between local stability and structure in glasses. We demonstrate the strength of this approach by applying our x-ray microscopy to colloidal glasses during aging and deformation.

We spatially resolve local structural stability by calculating the local time correlation coefficient, $C(\Delta t)$, obtained from the cross-correlation between μSAXS patterns taken with a time interval Δt [Fig. 1B and Materials and Methods (Eq. 4)]. This scanning μSAXS cross-correlation microscopy (*26*) maps local stability as the glass undergoes structural relaxations. We compare this local stability to two related, but distinct, measures of local structure: local centrosymmetry and local anisotropy. Local centrosymmetry probes disorder and divergence from perfectly centrosymmetric polyhedra in a dense, glassy assembly, while local anisotropy reflects volume-changing normal (ϵ_n) and volume-conserving shear (ϵ_s) distortions according to an anisotropy tensor.

We map the degree of local centrosymmetry in particle arrangements in a colloidal glass using "Friedel microscopy," which measures the breakdown in Friedel symmetry (or inversion symmetry (*27*)) in each scanning μSAXS pattern. This microscopy mode that has not been previously reported to our knowledge, probes the distribution of the magnitude of Ξ (fig. S8). Previous work has shown that the single-scattering approximation does not hold in general for thin, amorphous specimens (*28*). Limited probe-beam, multiply scattered speckle diffraction patterns (Fig. 1A) exhibit a lack of Friedel symmetry due to noncentrosymmetric particle arrangements, whereby the diffracted intensity at azimuthal angles ϕ and $\phi + \pi$ are not equivalent [$I(q, \phi) \neq I(q, \phi + \pi)$ for polar coordinates q and ϕ] (*25*, *29*–*32*). This breakdown in inversion symmetry in the diffraction pattern can be detected extremely sensitively from the appearance of odd symmetries in the angular autocorrelation function of the diffraction pattern (odd-order Fourier-coefficients $c^{2n+1} > 0$) [Fig. 1C and Materials and Methods (Eq. 3)] (*25*, *31*, *32*). On the basis of this, we propose here a parameter to quantify local structural centrosymmetry in glasses, which is the ratio of the even-to-odd angular symmetries in a μSAXS pattern ($\Sigma c^{2n+2}/\Sigma c^{2n+1}$; Materials and Methods).

The local in-plane normal and shear structural anisotropy (ϵ_n and ϵ_s) were derived by fitting the position of the first diffraction maximum in the μSAXS pattern with an anisotropy function, $\epsilon(\phi)$ [Fig. 1D and Materials and Methods (Eq. 5)], that measures the in-plane components of an anisotropy tensor (ϵ_{xx}, ϵ_{xy}, and ϵ_{yy}). These components are separated into the normal [$\epsilon_n = (\epsilon_{xx} + \epsilon_{yy})/2$] and shear

($\epsilon_s = \epsilon_{xy}$) components to map distortions in polyhedra resulting from local dilatation and contraction (positive and negative values of ϵ_n) and shear (ϵ_s). In some in situ experiments, this anisotropy has been related to the applied engineering strain (*33*, *34*). Here, this parameter represents local deviations from the average interparticle spacing.

Maps of these three parameters are derived solely from limited probe-beam diffraction patterns and provide many further opportunities to identify soft zones in glasses and understand their connection to local structures. Moreover, the size and distribution of soft zones can be directly determined, giving insight into their role in multiscale behaviors like aging, rejuvenation, and deformation. This diffraction-based method is an alternative to experimentally determining particle positions in three dimensions, which remains a considerable challenge for bulk glasses and the large volumes required to investigate multiscale phenomena (*35*, *36*).

RESULTS

Aging

Figure 2 shows maps of local stability [$C(\Delta t)$] and local structure in terms of the degree of centrosymmetry in local particle arrangements ($\Sigma c^{2n+2}/\Sigma c^{2n+1}$), and the in-plane normal and shear components of the structural anisotropy (ϵ_n, ϵ_s) measured from colloidal glasses that have been aged for 2 and 20 days (Fig. 2, A and B, respectively). The glasses are highly heterogeneous, with all the mapped parameters displaying an ostensibly random, snaking, and filamentous morphology. These heterogeneous regions persist and remain localized in the same area during relaxation (fig. S1) demonstrating dynamical heterogeneity (*37*). Examining histograms of the mapped parameters (Fig. 2C), we can distinguish the broad trends and different populations of structural states. Aging the glass increases local stability [$C(\Delta t)$] but decreases the average local degree of centrosymmetry ($\Sigma c^{2n+2}/\Sigma c^{2n+1}$). The shapes of distributions also change markedly, whereby the distribution of $\Sigma c^{2n+2}/\Sigma c^{2n+1}$ narrows and becomes symmetric, losing a small high-side shoulder, and at the same time, the stability [$C(\Delta t)$] and normal anisotropy (ϵ_n) broaden and develop a high-side shoulder. These observations paint a complex picture of aging that involves the reduction in centrosymmetry of local arrangements "frozen" in from the liquid phase and the separation into distinct regions with high/low centrosymmetry, anisotropy, and stability as the whole ensemble moves toward equilibrium (Fig. 1D). For these athermal systems, this involves maximizing vibrational entropy (*38*, *39*), which may provide the impetus behind the decrease in centrosymmetry and increase in normal anisotropy to produce the largest local volume for particles.

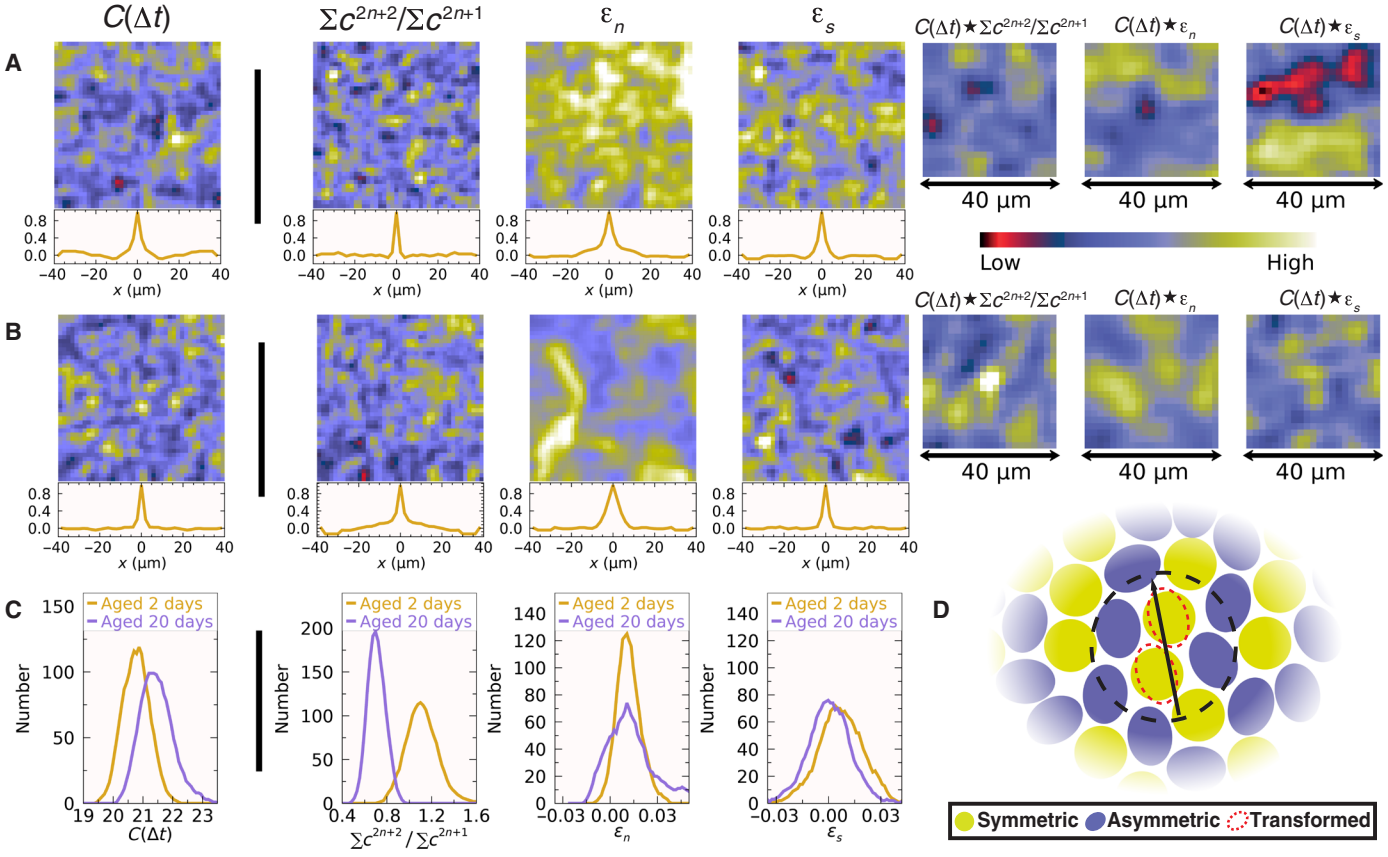

Fig. 2. Local stability and local structure of aged colloidal glasses. Local time correlation coefficient [$C(\Delta t)$], degree of centrosymmetry in local particle arrangements ($\Sigma c^{2n+2}/\Sigma c^{2n+1}$), and in-plane local anisotropy (ϵ_n, ϵ_s) of colloidal glasses that have been aged for (**A**) 2 days and (**B**) 20 days. Maps are scaled to display ± 4 SDs about the mean value. The anisotropy map scales are centered on zero. The radial average of the autocorrelation function of each map is plotted below the corresponding map. Cross-correlation functions (denoted with ⋆) are displayed on the right of the corresponding maps. (**C**) Histograms of mapped parameters. (**D**) Aging involves cooperative local transformations to lower symmetry structures.

Correlations within and between the mapped parameters confirm these trends. The radial average of the autocorrelation function is plotted below each map in Fig. 2, and the size of correlated domains can be estimated from the width of the central maxima in these functions. From these functions, we see that in the younger glass, all correlation lengths are limited to the spatial resolution of the probe (~7 μm) except the time correlation coefficient (see also fig. S2 and table S1). This observation and the smaller spread in the values of $C(\Delta t)$ suggest that the younger glass is more homogeneous, with local arrangements that have high/low centrosymmetry and high/low anisotropy intimately intermixed, producing less variation in stability. In contrast, the spatial correlation length of $C(\Delta t)$ decreases markedly with aging indicative of more distinct, spatially separated areas with fast and slow dynamics. Aging also induces a small increase in the correlation length of the local centrosymmetry (~11 polyhedra) and a larger increase in the size of the normal anisotropy field (~19 polyhedra), showing that fluctuating local order can produce longer-range cooperative displacements as anticipated by theory (*8*, *9*).

Cross-correlations between the local stability and the structural parameters are displayed in the rightmost panels of Fig. 2 (A and B) [$C(\Delta t) \star \Sigma c^{2n+2}/\Sigma c^{2n+1}$, $C(\Delta t) \star \epsilon_n$, $C(\Delta t) \star \epsilon_s$, where $\star$ denotes a cross-correlation as defined in Materials and Methods (Eq. 6)]. The spatial cross-correlation between local stability and local centrosymmetry is weakly positive for the young glass but greatly enhanced in the aged glass (see also fig. S3). The cross-correlation between stable local structures [high $C(\Delta t)$] and the anisotropy is negative for the younger glass indicative of the short-range strain fields. As the glass ages and larger domains with a dominant anisotropy emerge, this correlation becomes more positive. The local centrosymmetry parameter shows positive and negative spatial correlations with different components of the anisotropy (fig. S3), and these relationships strengthen with aging.

The complex relationship between the mapped parameters can be visualized further by plotting the distribution of the structural parameters that correspond to the different quartiles of the local stability as displayed in Fig. 3A, where we display the mean and SE. In the younger glass, the lowest quartile in stability associates with local configurations that have higher centrosymmetry than the second lowest quartile in stability. In contrast, in the aged glass, these unstable higher symmetry polyhedra have transformed to lower symmetry, and the plots show much stronger association between high stability and high centrosymmetry. The relationship of stability to anisotropy is reversed during aging, and the aged glass shows very pronounced positive relationships between $C(\Delta t)$ and ϵ_n and ϵ_s, respectively. This trend points to the central role of affine local structural transformations to create larger domains with a dominant anisotropy and reduced structural softness as illustrated in Fig. 2D.

Compression

Deformation also changes the magnitude and spatial distribution of the mapped parameters as can be seen in Fig. 4, where maps of the same area of a freshly prepared glass are compared before (Fig. 4A) and after (Fig. 4B) a compressive force is applied normal to the plane of the specimen. Examining histograms of the parameters (Fig. 4C), it is clear that while the average $C(\Delta t)$ has increased in the compressed specimen due to unavoidable aging during the experimental period (2 days), the distribution in the stability of local structures has broadened and become asymmetric with a low-stability shoulder. This contrasts to the distinct population of high-stability states that arose during the purely aging experiment (Fig. 2C). The degree of centrosymmetry in local structures has decreased

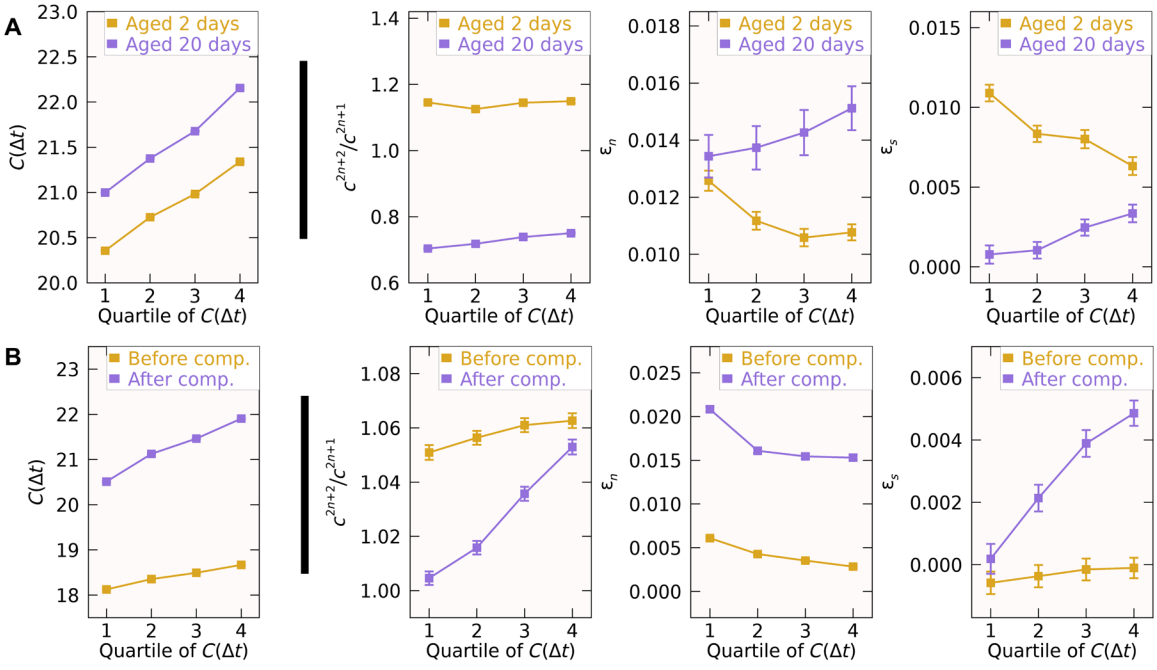

Fig. 3. Distributions of the local structure parameters that correspond to different quartiles of the local stability. The values of $\Sigma c^{2n+2}/\Sigma c^{2n+1}$, ϵ_n, and ϵ_s that correspond to the first, second, third, and fourth quartiles of $C(\Delta t)$ illustrated by the mean and the SEs for (**A**) the glasses aged for 2 and 20 days and (**B**) the glass before and after compression. The SE can be smaller than the data point.

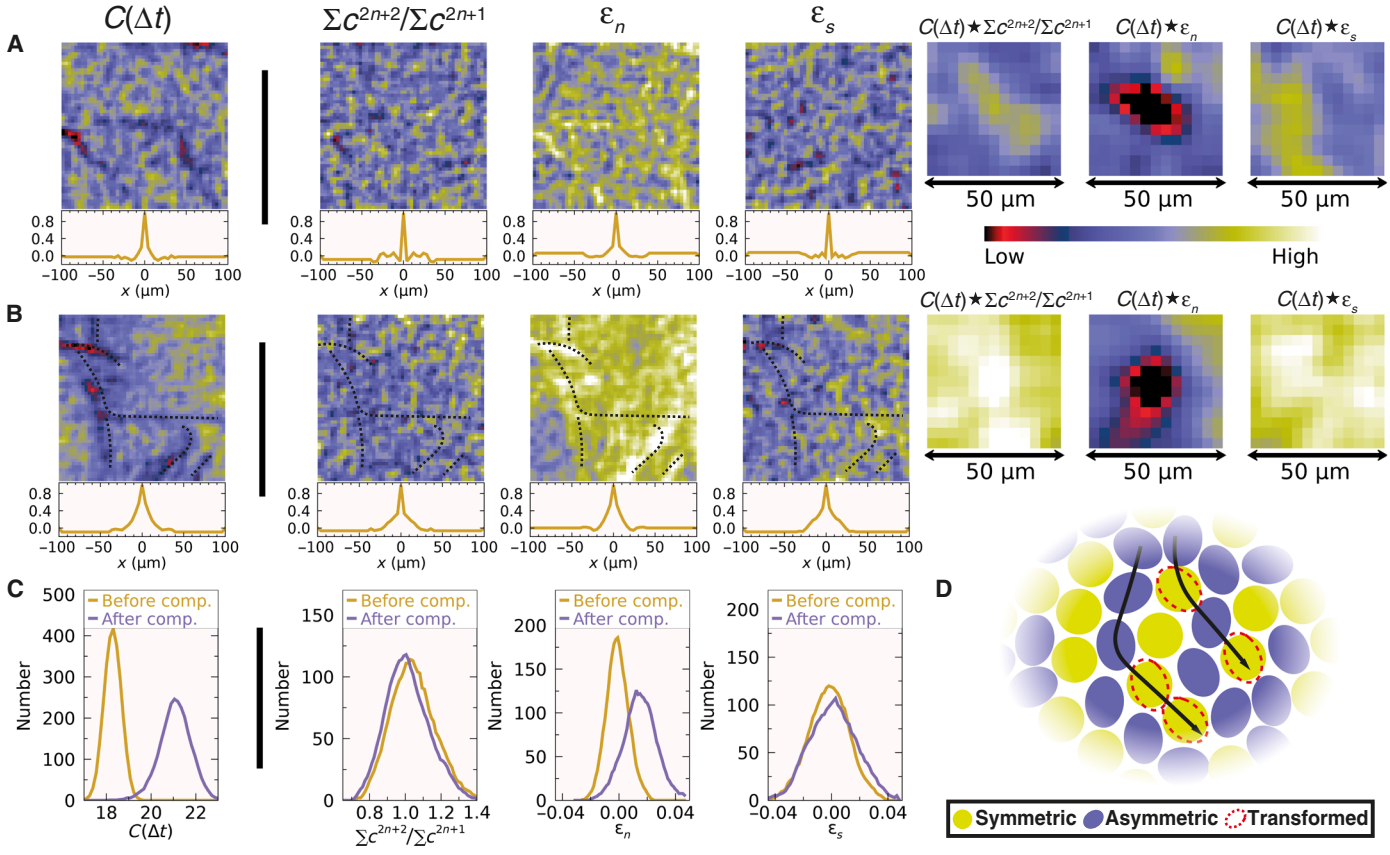

Fig. 4. Local stability and local structure of as-prepared and deformed colloidal glasses. Local time correlation coefficient [$C(\Delta t)$], degree of centrosymmetry in local particle arrangements ($\Sigma c^{2n+2}/\Sigma c^{2n+1}$) and in-plane local anisotropy (ϵ_n, ϵ_s) of (**A**) a fresh colloidal glass and (**B**) the same area after a compressive force has been applied. Maps are scaled to display ± 4 SDs about the mean value. The anisotropy map scales are centered on zero. The radial average of the autocorrelation function of each map is plotted below the corresponding map. Cross-correlation functions (denoted with ⋆) are displayed on the right of the corresponding maps. Note the increase in the scanned area compared to Fig. 2. Black dotted lines are drawn along bands with extremely low stability where anisotropy has localized. (**C**) Histograms of mapped parameters. (**D**) Deformation involves cooperative local transformations to lower symmetry structures in bands

only slightly, while the width of this distribution seems unaltered. In comparison to this, the distribution of normal anisotropy has broadened and developed asymmetries. The average value of ϵ_n has increased, indicating an overall generation of volume. This may seem unintuitive, but net dilatation caused by local structural transformations in disordered media is well known, even if the nature of the deformation is compressive (*40*).

It is quite remarkable how little the distribution of centrosymmetry in local arrangements changes for such a large increase in positive normal anisotropy. From the maps, the key point to explaining this phenomenon is the spatial connectedness of these transformations to lower symmetry (see Fig. 4D) and the emergence of low stability, high normal anisotropy "bands." The spatial connectedness of these regions is clearly evident by inspection and in increasing lateral correlation lengths. Before deformation, spatial correlations in the measured parameters do not extend very far (approximately seven polyhedra; see radial averaged autocorrelation functions below maps and fig. S4 and table S2). After deformation, the spatial correlation lengths of $C(\Delta t)$ and ϵ_n become much more extensive, even extending many hundreds of times the diameter of coordination polyhedra (fig. S4 and table S2). At the same time, the local degree of centrosymmetry develops two correlation lengths: a fluctuating one at the resolution limit, and a larger scale one, indicative of cooperative transformations in the bands. Inspecting the maps, we see that two distinct zones have emerged: one at the core of the bands where stability, centrosymmetry, and shear anisotropy are minimized and normal anisotropy is maximized, and surrounding this, a more diffuse region where these conditions decay spatially and contain short-range fluctuations. This observation supports previous measurements of softness and structure in and around a shear band that distinguish a localized core surrounded by broader, more diffuse zones (*41*, *42*). Our measurements show how a spatially fluctuating local centrosymmetry produces these highly cooperative and long-range displacements in shear bands (*8*, *9*, *43*). They further illuminate how localization plays a role in discontinuous yielding in amorphous materials (*44*).

Visual inspection of the maps and the calculated cross-correlation functions (rightmost panels of Fig. 4, A and B, and fig. S5) demonstrate that the spatial cross-correlations between parameters also strengthen from deformation. Deformation strengthens the spatial correlation between fast dynamics and low local centrosymmetry. It also strengthens the correlation between low $C(\Delta t)$ and large values of positive normal anisotropy. Comparing the areas in the compressed glass that show these clear trends (black overlaid dashed lines

in the Fig. 4B) to the same areas before compression is applied, potentially these shear bands initiate and propagate in areas where local particle arrangements are unstable and have low inversion symmetry. After deformation, these local arrangements, in turn, transform into yet more unstable, lower symmetry states, as illustrated in Fig. 4D.

These complex trends and the emergence of spatially localized bands of highly unstable, low centrosymmetry, and high normal anisotropy states can also be distinguished in the distributions of $\Sigma c^{2n+2}/\Sigma c^{2n+1}$ and anisotropy that correspond to the different quartiles of $C(\Delta t)$ as displayed in Fig. 3B. As for the aged glasses, it is clear that a large distribution of local structures corresponds to different dynamics, but distinct trends are present, whereby compression strengthens the relationship between low stability, low centrosymmetry, and high normal anisotropy. This is different from the relationship between symmetry and anisotropy produced by aging, perhaps indicative of the relative importance of affine, volume conserving shear structural transformations in aging, and nonaffine volume generating normal structural transformations in deformation. Another possible explanation for this observation is that aging and compression in this experiment involved long-range overall/applied stress in the plane of the specimen and perpendicular to this, respectively.

DISCUSSION

We have demonstrated a firm link between the spatial distribution of structural stability and the centrosymmetry of local particle arrangements in a colloidal glass. When coupled with spatially resolved measurements of local anisotropy, these maps provide a more complete understanding of the effects of aging and deformation on particle-scale structure and softness. These measurements are a quantitative bridge between local structure and global phenomena, confirming theoretical predictions that relate local structural symmetry to larger-scale, cooperative behavior. As anticipated by theory, the parameters that probed the local degree of inversion symmetry in the glasses were short-range and fluctuating with a seemingly random filamentous structure. Aging and deformation both involved reductions in the local structural centrosymmetry of quenched-in polyhedra. Larger-scale, cooperative behavior was produced by the spatial connectedness of these local structural transformations. Our measurements reveal that the key relationship in understanding multiscale phenomena such as aging and mechanical deformation in dense, glassy assemblies of particles is the connection between local structure and structural stability. This link between structure and behavior in glasses provides further opportunities to understand aging, rejuvenation, deformation, and failure and engineer tougher glasses from the particle level. While this contribution used an x-ray microbeam to probe colloidal microspheres, the probe beam could readily be tuned to investigate universal glassy phenomena across decades in length scale, ranging from nanobeam electron diffraction for atomic glasses to millibeam coherent light scattering for granular packings.

MATERIALS AND METHODS

μSAXS patterns were obtained by scanning a specimen with an ultralow divergence 5.5-keV x-ray beam shaped by cleaved Ge slits (*45*) and limited by a near-field aperture (7 μm diameter in tungsten, Lennox Laser, MD, USA). The 300-nm-diameter colloidal SiO_2 glass specimens (polydispersity 5%, Bangs Labs, IN, USA) were sandwiched between two 15-μm Kapton polymer film layers with a spacer layer to control the thickness to 20 μm. The controlled thickness and near-field aperture limit the number of polyhedral clusters that contribute to each diffraction pattern and give rise to well-resolved "speckles" (fig. S6) (*31*, *32*). The limited thickness also simplifies the interpretation of odd symmetries in the diffraction pattern as discussed further below. Specimen scans were conducted with 2-μm steps for the aging experiments and 4-μm steps for the in situ compression experiment over larger areas. Diffraction patterns were collected using a Dectris - Pilatus 1 M direct detection camera at a camera length of 7244 mm, giving rise to measurements of $I(q_x, q_y, x, y)$ at different scattering angles defined by q_x and q_y and positions (x, y). A novel spatiotemporal scan strategy was used to investigate local dynamics whereby the same matrix of (x, y) points was scanned several times to enable the magnitude of local structural variations to be probed as a function of time. This produced sets of $I(q_x, q_y, x, y, t)$ and $I(q_x, q_y, x, y, t + \Delta t)$ from which a local time correlation coefficient could be calculated with Δt = 1040 s for the aged glasses and Δt = 2250 s for the deformed glasses with larger area scans.

The particles were dispersed in water. Repulsive interparticle potentials were screened using salt (0.1 M NaCl). Further details of colloidal dispersion preparation have been reported previously (*23*). Dispersions (2.5%) were centrifuged into glasses for 10 min at 10,000 rpm in an Eppendorf miniSpin and immediately encapsulated between the Kapton films in the specimen holder and sealed. Glasses were aged in the specimen holder between the Kapton sheets. A compressive force was applied to encapsulated glasses by evenly compressing a 2-mm-diameter area between two cylindrical metal posts.

The angular autocorrelation function $[C(q, \Delta)]$ of each diffraction pattern $[I(q_x, q_y, x, y) = I(q, \phi)]$ is calculated according to

$$C(q,\Delta) = \left(\left\langle I(q,\phi)\, I(q,\phi+\Delta)\right\rangle_\phi - \left\langle I(q,\phi)\right\rangle_\phi^2\right) / \left\langle I(q,\phi)\right\rangle_\phi^2 \qquad (3)$$

Here, $|\boldsymbol{q}| = q = \sqrt{q_x^2 + q_y^2} = 4\pi\sin\theta/\lambda$ is the scattering vector magnitude, where θ is the scattering angle, and λ is the x-ray wavelength. ϕ is the azimuthal angle in the diffraction plane. $\langle X\rangle_\phi = \frac{1}{2\pi}\int_0^{2\pi} X d\phi$ denotes averaging over the azimuthal angle ϕ. Normalized symmetry magnitudes c_q^n/c_q^0 are calculated by Fourier decomposition of the angular autocorrelation (*46*) at each value of q. The average of these normalized symmetry magnitudes from a q range corresponding to the first peak in the structure factor located at q_1 ($c^n/c^0 = < c_q^n/c_q^0 >_{q1}$) is used to probe the angular symmetry in local polyhedral particle arrangements (fig. S7).

These Fourier coefficients include odd symmetries (*31*, *32*). The presence of these symmetries indicates a breakdown in Friedel symmetry or the nonequivalency in diffracted intensities that are related by inversion or equivalently, an angular rotation of π (*31*, *32*). There are three main sources of this Friedel symmetry breakdown, which are a probe beam with an imaginary component, Ewald sphere curvature, and dynamical diffraction from an object without a center of symmetry in the transverse direction (*29*–*32*). In this case, the probe beam over the 7-μm-diameter aperture is real to a high degree. The magnitude of the Ewald sphere curvature for 5.5 keV x-rays at the scattering angles studied is 10 times smaller than the inverse of the specimen thickness, and so, Ewald sphere curvature does not contribute appreciably to the observed breakdown in Friedel symmetry. Thus, the observed asymmetry in the magnitude of opposing diffracted intensities can be ascribed to dynamical diffraction from

particles with a noncentrosymmetric in-plane arrangement within the near-field aperture.

On the basis of this observation, we propose and measure a parameter to quantify the degree of centrosymmetry of local structures. This is $\Sigma c^{2n+2}/\Sigma c^{2n+1}$ for $0 \leq n \leq 5$, which will probe the degree of centrosymmetry in the plane perpendicular to the beam direction as shown in soft x-ray dynamical diffraction simulations (*47*) (fig. S8) using tabulated values for the complex refractive index of the SiO_2 spheres (*48*). X-ray scatter from the aperture produces some structure in the incident beam, resulting in a low level of streaking in the μSAXS patterns of the glass (fig. S6). This contribution will be approximately constant in the centrosymmetry ratios calculated, and thus, the mapped parameters reflect the centrosymmetry in the local structure of the glass at different positions.

The local time correlation coefficient at each point in the scanned array (x, y) was calculated from the intensity $[I(q_x, q_y, x, y, t) = I(t)]$ according to

$$C(\Delta t) = \left\langle \left(I(t) - \langle I(t)\rangle_{q1}\right)\left(I(t+\Delta t) - \langle I(t+\Delta t)\rangle_{q1}\right)\right\rangle_{q1} / \left(\langle I(t)\rangle_{q1}\langle I(t+\Delta t)\rangle_{q1}\right) \quad (4)$$

This is similar in principle to x-ray photon cross-correlation spectroscopy (*49*, *50*) but with the key difference of using a small near-field aperture to examine local dynamics in a limited area (*26*). The local dynamics vary from point-to-point, enabling the heteogeneity in local structural dynamics in the glass to be visualized (fig. S9).

The local structural anisotropy was calculated by dividing the diffracted intensity into arcs with an angular range of π/24 and averaging the diffracted intensity in these arcs over the azimuthal angle of π/24. The center of mass of the average diffracted intensity from each arc was calculated to give a value of $q_{\max}$ corresponding to the scattering vector where the peak in the diffracted intensity is located. The local anisotropy was obtained by normalizing this by the average $q_0 = \langle q_{\max}\rangle_\phi$ from the average μSAXS pattern of the entire ensemble. The local function was fitted to extract the components of the normal and shear anisotropy (*33*, *34*) in the plane of the specimen as follows (fig. S10)

$$\epsilon(\phi) = (q_0 - q_{\max}(\phi))/q_{\max}(\phi) = \epsilon_{xx}\cos^2(\phi) + \epsilon_{xy}\cos(\phi)\sin(\phi) + \epsilon_{yy}\sin^2(\phi) \quad (5)$$

Values of q_0 were determined from the averaged μSAXS pattern for the two aged glasses so that the mapped anistropy is the local deviation from the average. For the compression experiments, q_0 was determined from the averaged diffraction pattern for the glass before compression. Normal and shear in-plane components are displayed: $\epsilon_n = (\epsilon_{xx} + \epsilon_{yy})/2$ and $\epsilon_{xy} = \epsilon_s$. Thus, a positive value for ϵ_n indicates dilatation, while ϵ_s is a volume conserving anisotropy. Here, we refer to these parameters as reflecting the local structural anisotropy, but in previous large and small probe diffraction measurements, they have been related to the applied engineering strain (*33*, *34*).

Maps were smoothed using a Savitsky-Golay (*51*) smoothing kernel with a width of 4 and an order of 2. This optimal least-squares fitting method smooths noise while retaining the width and magnitude of peaks (fig. S11).

The autocorrelation and cross-correlation of maps was calculated according to

$$\left[f(x,y) \star g(x,y)\right](\Delta x, \Delta y) = \left\langle \left(f(x,y) - \langle f(x,y)\rangle_{x,y}\right)\left(g(x+\Delta x, y+\Delta y) - \left\langle g(x,y)\right\rangle_{x,y}\right)\right\rangle_{x,y} / (\sigma_{f(x,y)}\sigma_{g(x,y)}) \quad (6)$$

where the normalization by the standard deviations $\sigma_{f(x,y)}\sigma_{g(x,y)}$ ensures the correlations range from 1 for perfect correlation and −1 for perfect anticorrelation.

The application of the Savitsky-Golay filter did not increase the extent of any measured correlation as shown in fig. S11, where the filtered autocorrelation is compared to the unfiltered result. The major and minor full width half maxima of the central correlation were extracted by using an elliptical Gaussian curve fit (tables S1 and S2).

SUPPLEMENTARY MATERIALS

Supplementary material for this article is available at https://science.org/doi/10.1126/sciadv.abn0681

REFERENCES AND NOTES

1. C. P. Royall, S. R. Williams, The role of local structure in dynamical arrest. *Phys. Rep.* **560**, 1–75 (2015).
2. D. Richard, M. Ozawa, S. Patinet, E. Stanifer, B. Shang, S. A. Ridout, B. Xu, G. Zhang, P. K. Morse, J.-L. Barrat, L. Berthier, M. L. Falk, P. Guan, A. J. Liu, K. Martens, S. Sastry, D. Vandembroucq, E. Lerner, M. L. Manning, Predicting plasticity indisordered solids from structural indicators. *Phys. Rev. Mater.* **4**, 113609 (2020).
3. E. D. Cubuk, R. J. S. Ivancic, S. S. Schoenholz, D. J. Strickland, A. Basu, Z. S. Davidson, J. Fontaine, J. L. Hor, Y.-R. Huang, Y. Jiang, N. C. Keim, K. D. Koshigan, J. A. Lefever, T. Liu, X.-G. Ma, D. J. Magagnosc, E. Morrow, C. P. Ortiz, J. M. Rieser, A. Shavit, T. Still, Y. Xu, Y. Zhang, K. N. Nordstrom, P. E. Arratia, R. W. Carpick, D. J. Durian, Z. Fakhraai, D. J. Jerolmack, D. Lee, J. Li, R. Riggleman, K. T. Turner, A. G. Yodh, D. S. Gianola, A. J. Liu, Structure-property relationships from universal signatures of plasticity in disordered solids. *Science* **358**, 1033–1037 (2017).
4. S. Schoenholz, E. Cubuk, D. Sussman, E. Kaxiras, A. J. Liu, A structural approach to relaxation in glassy liquids. *Nat. Phys.* **12**, 469–471 (2016).
5. S. Ketov, Y. Sun, S. Nachum, Z. Lu, A. Checchi, A. R. Beraldin, H. Y. Bai, W. H. Wang, D. V. Louzguine-Luzgin, M. A. Carpenter, A. L. Greer, Rejuvenation of metallic glasses by nonaffine thermal strain. *Nature* **254**, 200–203 (2015).
6. R. Milkus, A. Zaccone, Local inversion-symmetry breaking controls the boson peak in glasses and crystals. *Phys. Rev. B* **93**, 094204 (2016).
7. M. Schlegel, J. Brujic, E. M. Terentjev, A. Zaccone, Local structure controls the nonaffine shear and bulk moduli of disordered solids. *Sci. Rep.* **6**, 18724 (2016).
8. A. Lemaître, C. Maloney, Sum rules for the quasi-static and visco-elastic response of disordered solids at zero temperature. *J. Stat. Phys.* **123**, 415–453 (2006).
9. C. Maloney, A. Lemaître, Amorphous systems in athermal, quasistatic shear. *Phys. Rev. E* **74**, 016118 (2006).
10. A. Zaccone, E. Scossa-Romano, Approximate analytical description of the nonaffine response of amorphous solids. *Phys. Rev. B* **83**, 184205 (2011).
11. M. L. Falk, J. S. Langer, Dynamics of viscoplastic deformation in amorphous solids. *Phys. Rev. E* **57**, 7192–7205 (1998).
12. P. Morse, S. Wijtmans, M. van Deen, M. van Hecke, M. L. Manning, Differences in plasticity between hard and soft spheres. *Phys. Rev. Res.* **2**, 023179 (2020).
13. G. L. Hunter, E. R. Weeks, The physics of the colloidal glass transition. *Rep. Prog. Phys.* **75**, 066501 (2012).
14. T. Kawasaki, H. Tanaka, Structural evolution in the aging process of supercooled colloidal liquids. *Phys. Rev. E* **89**, 062315 (2014).
15. A. Greer, Y. Q. Cheng, E. Ma, Shear bands in metallic glasses. *Mater. Sci. Eng. R* **74**, 71–132 (2013).
16. V. Chikkadi, G. Wegdam, D. Bonn, B. Nienhuis, P. Schall, Long-range strain correlations in sheared colloidal glasses. *Phys. Rev. Lett.* **107**, 198303 (2011).
17. P. Schall, D. A. Weitz, F. Spaepen, Structural rearrangements that govern flow in colloidal glasses. *Science* **318**, 1895–1899 (2007).
18. K. E. Jensen, D. A. Weitz, F. Spaepen, Local shear transformations in deformed and quiescent hard-sphere colloidal glasses. *Phys. Rev. E* **90**, 042305 (2014).
19. B. Li, K. Lou, W. Kob, S. Granick, Anatomy of cage formation in a two-dimensional glass-forming liquid. *Nature* **587**, 225–229 (2020).

20. M. Clusel, E. I. Corwin, A. O. N. Siemens, J. Brujic, A "granocentric" model for random packing of jammed emulsions. *Nature* **460**, 611–615 (2009).
21. N. C. Keim, J. D. Paulsen, Multiperiodic orbits from interacting soft spots in cyclically sheared amorphous solids. *Sci. Adv.* **7**, 7685 (2021).
22. A. A. Zadeh, J. Barés, T. A. Brzinski, K. E. Daniels, J. Dijksman, N. Docquier, H. O. Everitt, J. E. Kollmer, O. Lantsoght, D. Wang, M. Workamp, Y. Zhao, H. Zheng, Enlightening force chains: A review of photoelasticimetry in granular matter. *Granul. Matter* **21**, 83 (2019).
23. A. C. Y. Liu, R. F. Tabor, M. D. de Jonge, S. T. Mudie, T. C. Petersen, Favored local structures in amorphous colloidal packings measured by microbeam X-ray diffraction. *Proc. Natl. Acad. Sci.* **114**, 10344–10349 (2017).
24. P. Wochner, C. Gutt, T. Autenrieth, T. Demmer, V. Bugaev, A. D. Ortiz, A. Duri, F. Zontone, G. Grübel, H. Dosch, X-ray cross correlation analysis uncovers hidden local symmetries in disordered matter. *Proc. Natl. Acad. Sci.* **106**, 11511–11514 (2009).
25. E. D. Bøjesen, T. C. Petersen, A. V. Martin, M. Weyland, A. C. Y. Liu, Statistical measures of angular correlations in amorphous materials from electron nano-diffraction in the scanning/transmission electron microscope. *J. Phys. Mater.* **3**, 044002 (2020).
26. M. M. Hurley, P. Harrowell, Resolving the structural relaxation of a two-dimensional liquid using apertured cross correlation functions. *J. Chem. Phys.* **107**, 8586–8593 (1997).
27. U. Shmueli, H. D. Flack, J. C. H. Spence, Methods of space-group determination, in *International Tables for Crystallography A* , M. I. Aroyo, Ed. (IUCr, 2016), chap. 1.6, pp. 107–131.
28. G. R. Anstis, Z. Liu, M. Lake, Investigation of amorphous materials by electron diffraction - the effects of multiple scattering. *Ultramicroscopy* **26**, 65–69 (1988).
29. J. M. Rodenburg, Properties of electron microdiffraction patterns from amorphous materials. *Ultramicroscopy* **25**, 329–343 (1988).
30. M. J. Hÿtch, J. P. Chevalier, On the breakdown of Friedel's Law for coherent microdiffraction from amorphous materials. *Ultramicroscopy* **58**, 114–121 (1995).
31. A. C. Y. Liu, G. R. Lumpkin, T. C. Petersen, J. Etheridge, L. Bourgeois, Interpretation of angular symmetries in electron nanodiffraction patterns from thin amorphous specimens. *Acta Crystallogr. Sect. A* **71**, 473–482 (2015).
32. A. C. Y. Liu, R. F. Tabor, L. Bourgeois, M. D. de Jonge, S. T. Mudie, T. C. Petersen, Probing local order in glasses from limited-volume electron and x-ray diffraction. *J. Stat. Mech. Theor. Exp.* **2016**, 054046 (2016).
33. R. T. Ott, M. I. Mendelev, M. F. Besser, M. J. Kramer, J. Almer, D. J. Sordelet, Strain dependence of peak widths of reciprocal- and real-space distribution functions of metallic glasses from in situ x-ray scattering and molecular dynamics simulations. *Phys. Rev. B* **80**, 064101 (2009).
34. T. C. Pekin, J. Ding, C. Gammer, B. Ozdol, C. Ophus, M. Asta, R. O. Ritchie, A. M. Minor, Direct measurement of nanostructural change during in situ deformation of a bulk metallic glass. *Nat. Commun.* **10**, 2445 (2019).
35. Y. Yang, J. Zhou, F. Zhu, Y. Yuan, D. J. Chang, D. S. Kim, M. Pham, A. Rana, X. Tian, Y. Yao, S. J. Osher, A. K. Schmid, L. Hu, P. Ercius, J. Miao, Determining the three-dimensional atomic structure of an amorphous solid. *Nature* **592**, 60–64 (2021).
36. T. Aste, M. Saadatfar, A. Sakellariou, T. Senden, Investigating the geometrical structure of disordered sphere packings. *Phys. A: Stat. Mech. Appl.* **339**, 16–23 (2004).
37. F. Corberi, L. F. Cugliandolo, H. Yoshino, Growing length scales in aging systems, in *Dynamical Heterogeneities in Glasses, Colloids and Granular Media* , L. Berthier, G. Biroli, J.-P. Bouchaud, L. Cielletti, W. van Saarloos, Ed. (Oxford UP Oxford, 2011), chap. 11, pp. 370–401.
38. G. C. Cianci, R. E. Courtland, E. R. Weeks, Correlations of structure and dynamics in an aging colloidal glass. *Solid State Commun.* **139**, 599–604 (2006).
39. H. Tanaka, H. Tong, R. Shi, J. Russo, Revealing key structural features hidden in liquids and glasses. *Nat. Rev. Phys.* **1**, 333–348 (2019).
40. F. Spaepen, Must shear bands be hot? *Nat. Mater.* **5**, 7–8 (2006).
41. R. Maaß, K. Samwer, W. Arnold, C. A. Volkert, A single shear band in a metallic glass: Local core and wide soft zone. *Appl. Phys. Lett.* **105**, 171902 (2014).
42. R. Maaß, P. Birckigt, C. Borchers, K. Samwer, C. A. Volkert, Long range stress fields and cavitation along a shear band in a metallic glass: The local origin of fracture. *Acta Mater.* **98**, 94–102 (2015).
43. M. Baggioli, I. Kriuchevskyi, T. W. Sirk, A. Zaccone, Plasticity in amorphous solids is mediated by topological defects in the displacement. *Phys. Rev. Lett.* **127**, 015501 (2021).
44. M. Ozawa, L. Berthier, G. Biroli, A. Rosso, G. Tarjus, Random critical point separates brittle and ductile yielding transitions in amorphous materials. *Proc. Natl. Acad. Sci.* **115**, 6656–6661 (2018).
45. N. M. Kirby, S. T. Mudie, A. M. Hawley, D. J. Cookson, H. D. T. Mertens, N. Cowieson, V. Samardzic-Boban, A low-background-intensity focusing small-angle X-ray scattering undulator beamline. *J. Appl. Crystallogr.* **46**, 1670–1680 (2013).
46. A. C. Y. Liu, R. F. Tabor, L. Bourgeois, M. D. de Jonge, S. T. Mudie, T. C. Petersen, Calculation of projected bond-orientational order parameters to quantify local symmetries from transmission diffraction data. *Phys. Rev. Lett.* **116**, 205501 (2016).
47. A. R. Hare, G. R. Morrison, Near-field soft X-ray diffraction modelled by the multislice method. *J. Mod. Opt.* **41**, 31–48 (1994).
48. B. Henke, E. Gullikson, J. Davis, X-ray interactions: Photoabsorption, scattering, transmission, and reflection at E = 50-30,000 eV, Z = 1-92. *At. Data Nucl. Data Tables* **54**, 181–342 (1993).
49. A. R. Sandy, Q. Zhang, L. B. Lurio, Hard X-Ray photon correlation spectroscopy methods for materials studies. *Annu. Rev. Mater. Res.* **48**, 167–190 (2018).
50. O. G. Shpyrko, X-ray photon correlation spectroscopy. *J. Synchrotron Radiat.* **21**, 1057–1064 (2014).
51. M. Savitzky, J. E. Golay, Smoothing and differentiation of data by simplified least squares procedures. *Anal. Chem.* **36**, 1627–1639 (1964).

Acknowledgments: This research was undertaken on the SAXS/WAXS beamline at the Australian Synchrotron, Victoria, Australia. We thank J. Etheridge, L. Bourgeois, D. Paganin, T. Davis, and A. Martin for discussions. **Funding:** A.C.Y.L. acknowledges support from the Monash Centre for Electron Microscopy and the Australian Research Council (FT180100594). E.D.B. acknowledges financial support from the Villum Foundation (VKR023371) and the Australian Research Council (DP150104483). **Author contributions:** A.C.Y.L., R.F.T., T.C.P., S.T.M., and E.D.B. performed the experiment. A.C.Y.L. conducted the data analysis and manuscript preparation with contributions from all the other authors. All authors contributed to the conception of the experiment and interpretation of results. **Competing interests:** The authors declare that they have no competing interests. **Data and materials availability:** All data needed to evaluate the conclusions in the paper are present in the paper and/or the Supplementary Materials. Datasets are available at https://doi.org/10.26180/17209553.

Submitted 1 November 2021
Accepted 21 January 2022
Published 18 March 2022
10.1126/sciadv.abn0681

ScienceAdvances

Local symmetry predictors of mechanical stability in glasses

Amelia C. Y. LiuEspen D. BøjesenRico F. TaborStephen T. MudieAlessio ZacconePeter HarrowellTimothy C. Petersen

Sci. Adv., 8 (11), eabn0681.

Science Advances (ISSN) is published by the American Association for the Advancement of Science. 1200 New York Avenue NW, Washington, DC 20005. The title *Science Advances* is a registered trademark of AAAS.